Intramolecular Interligand Charge Transfer in Hexacoordinate Silicon Complexes

Jörg Wagler,* Daniela Gerlach, Uwe Böhme, and Gerhard Roewer

Institut für Anorganische Chemie, Technische Universität Bergakademie Freiberg, Leipziger Strasse 29, D-09596 Freiberg, Germany

Received September 21, 2005

The linking of amide and imine ligands in the coordination sphere of octahedral silicon complexes opens access to new compounds with intense interligand charge transfer. In these novel complexes the highest occupied MOs are located around the amide nitrogen atoms, while the imine moieties significantly contribute to the formation of LUMO and LUMO+1 and the hexacoordinate silicon atom plays an important role in bridging these donor and acceptor sites. Regarding the intensity of the CT, the architecture of the silicon coordination sphere plays a dominant role: the trans situation between the amide and imine ligand donor atoms provides a much more favored CT than is found in a *trans*-(imine, imine)-*cis*-(imine, amide) complex.

Introduction

Hypercoordinate silicon complexes have captured the interest of academic and industrial laboratories, due to their potential in developing pathways for the synthesis of chemicals which may otherwise be difficult to prepare or even be inaccessible. Thus, bond activation by hypercoordination[1] or, in the opposite sense, the prevention of nucleophilic substitutions at the Si atom by blocking nucleophile-accessible sites with donor atoms[2] is worth mentioning. Electronic properties and reactivities of molecules bearing silicon atoms can be significantly changed by switching the coordination number of the Si atom. Oligosilanes bearing pentacoordinate Si atoms are known to exhibit bathochromically shifted UV absorptions.[3] The addition of a fluoride ion to trianthrylfluorosilane creates a silicate which is fluorescent,[4] and as recently reported, even photochemically induced reactions such as Si−C bond cleavage can be promoted by hexacoordination of the silicon atom involved.[5] Vice versa, the coordination sphere around Si atoms can be triggered by photochemical impact.[6] However, it has been widely unexplored whether there are some significant influences of the hypercoordinate Si atom's coordination environment on the respective compound's visible spectra. Usually the silicon complexes are colorless, except when the Si atom is coordinated by colored ligand systems such as phthalocyanines and porphyrins.[7] The Si atom, however, may link such ligands that exhibit donor and acceptor qualities to each other. Thus, accomplishing this coupling enables electronic interaction between such ligands. It has long been a dream to synthesize such colored silicon compounds exhibiting intense low-energy light absorption. Recently, Driess et al. discussed intramolecular charge-transfer effects in a novel kind of hypercoordinate Si complex.[8] The complexes presented in their paper, however, were colorless compounds.

We now report the phenomenon of low-energy interligand charge transfer via the hexacoordinate silicon atom in Si complexes with a mixed coordination sphere which is built upon ligands of the anilide and 2-(iminomethyl)phenolate types.

Scheme 1. Linking of Electron Donor (Blue) and Acceptor Sites (Red) via the Hexacoordinate Silicon Atom

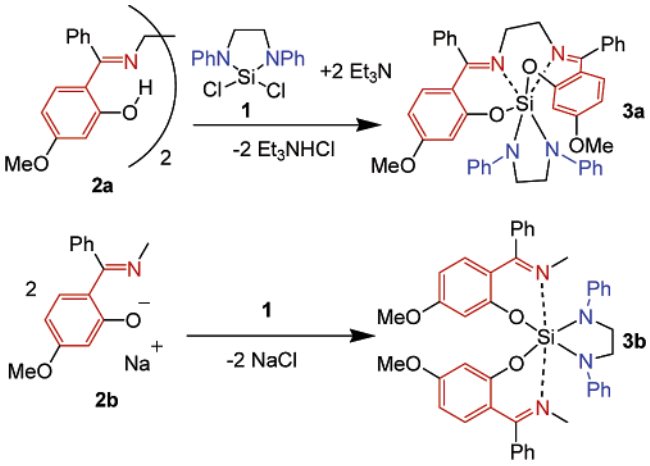

Results and Discussion

Usually coordination of salen-type ligands at the Si atom gives rise only to a slightly shifted UV/vis absorption, depending on the strength of the N→Si coordination and the Lewis acidity of the silicon atom, which affect the electronic properties of the

* To whom correspondence should be addressed. Tel: (+49) 3731 39 3556 or (+49) 3731 39 4343. Fax: (+49) 3731 39 4058. E-mail: joerg.wagler@chemie.tu-freiberg.de.

(1) For example see: (a) Wagler, J.; Böhme, U.; Roewer, G. *Organometallics* **2004**, *23*, 6066. (b) Chopra, S. K.; Martin, J. C. *J. Am. Chem. Soc.* **1990**, *112*, 5342. (c) Berger, R.; Duff, K.; Leighton, J. L. *J. Am. Chem. Soc.* **2004**, *126*, 5686. (d) Chuit, C.; Corriu, R. J. P.; Reye, C.; Young, J. C. *Chem. Rev.* **1993**, *93*, 1371.

(2) Kobayashi, J.; Ishida, K.; Kawashima, T. *Silicon Chem.* **2002**, *1*, 351.

(3) El-Sayed, I.; Hatanaka, Y.; Onozawa, S.; Tanaka, M. *J. Am. Chem. Soc.* **2001**, *123*, 3597.

(4) Yamaguchi, S.; Akijama, S.; Tamao, K. *J. Organomet. Chem.* **2002**, *652*, 3.

(5) Wagler, J.; Doert, Th.; Roewer, G. *Angew. Chem., Int. Ed.* **2004**, *43*, 2441.

(6) Kano, N.; Komatsu, F.; Kawashima, T. *J. Am. Chem. Soc.* **2001**, *123*, 10778.

(7) (a) Ishii, K.; Takeuchi, S.; Shimizu, S.; Kobayashi, N. *J. Am. Chem. Soc.* **2004**, *126*, 2082. (b) Kane, K. M.; Lorenz, C. R.; Heilman, D. M.; Lemke, F. R. *Inorg. Chem.* **1998**, *37*, 669.

(8) Driess, M.; Muresan, N.; Merz, K.; Paech, M. *Angew. Chem., Int. Ed.* **2005**, *44*, 6738.

10.1021/om050816e CCC: $33.50
Publication on Web 05/03/2006

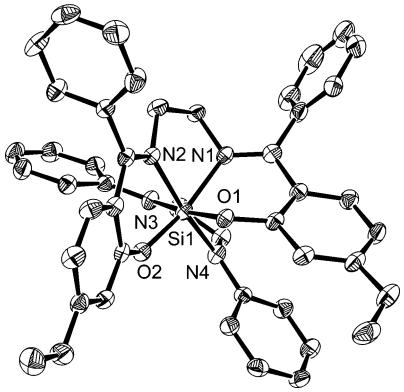

Figure 1. Molecular structure of **3a** in the crystal[12] of **3a**·2(dioxane) (ORTEP plot, 50% probability ellipsoids, hydrogen atoms and dioxane molecules omitted for clarity).

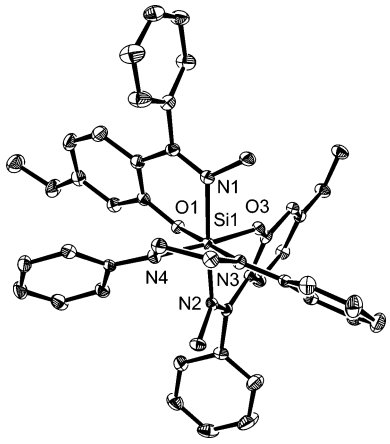

Figure 2. Molecular structure of one of the two crystallographically independent molecules of **3b** in the crystal[12] (ORTEP plot, 50% probability ellipsoids, hydrogen atoms omitted for clarity).

C═N moiety. Thus, the yellowish color of salen-type ligands is mostly retained in related silicon complexes.[9] Even a distortion to a *mer-fac*-arranged salen moiety in the hexacoordinate Si complex **I**[10] as a result of the complexation of a silacycle does not cause any severe effects on its visible spectra (see Figure 3).

To stimulate low-energy electronic transitions in such silicon complexes, 1,1-dichloro-2,5-diphenyl-2,5-diazasilolidine (**1**)[11] was reacted with the tetradentate salen-type ligand **2a** in the presence of triethylamine to yield **3a**. Surprisingly, this hexacoordinate silicon complex (Scheme 1, Figure 1) exhibits a remarkably intense red color.

Reaction of the sodium salt of the bidentate 2-(iminomethyl)-phenolate ligand **2b** together with **1** also resulted in the formation of a complex bearing a hexacoordinate Si atom, **3b** (Scheme 1; Figure 2). In contrast with the intense color of **3a**, this compound is only a lighter orange.

The coordination sphere around the Si atom in **3a** is distorted octahedral. The Si−N bonds to the imine nitrogen atoms (Si1−N1 = 1.989(2) Å, Si1−N2 = 1.964(2) Å) are significantly longer than those to the amide N atoms (Si1−N3 = 1.833(2) Å, Si1−N4 = 1.806(2) Å). However, the Si−N(imine) and the Si−N(amide) bonds have similar lengths, respectively, while the Si−O bonds (Si1−O1 = 1.786(1) Å, Si1−O2 = 1.730(1) Å) exhibit notable differences. The silicon atom is localized in a slight out-of-plane position from the chelate N2−C−C−C−O2 (0.624(2) Å) while it is remarkably out of plane in the N1−C−C−C−O1 chelate (0.911(2) Å). The phenyl groups attached to the salen ligand system are almost perpendicularly arranged with respect to the nearest [Si−N−C−C−C−O] chelate, but in contrast, those connected to the diazasilolidine ring system are in plane with the planar environments of the amide N atoms.

The crystal structure of **3b** consists of two crystallographically independent molecules which significantly differ in the orientation of the methoxy and phenyl substituents at one of the two bidentate O,N-ligand moieties. The arrangements of the donor atoms in the Si coordination spheres are quite equal. Thus, only one of those molecules is depicted in Figure 2 and discussed herein. Interestingly, despite the nearly C_s symmetry of molecule **3b**, the Si−N(imine) bond lengths (Si1−N1 = 2.006(2) Å, Si1−N2 = 1.939(2) Å) differ even more than in the rather asymmetric molecule **3a**. The Si−N(amide) (Si1−N3 = 1.827(2) Å, Si1−N4 = 1.833(2) Å) and Si−O bonds (Si1−O1 = 1.766(2) Å, Si1−O3 = 1.762(1) Å), however, have the same lengths, respectively. The longer Si−N(imine) bond Si1−N1 is expected to result from steric repulsion between the imine moiety of the half salen ligand and the CH_2−CH_2 bridge of the diazasilolidine ring system, which is folded toward atom N1. Vice versa, the bond Si1−N2 should be shorter, due to the lack of this repulsion.

The arrangement of the nitrogen atoms in the coordination sphere of the Si atom does cause the striking difference between the molecular architectures of **3a** and **3b**. In **3a** the salen-type ligand is in a *mer-fac* arrangement, a configuration which has been found to be more stable than the *fac-fac* arrangement.[13] In this complex an amide N atom (N4) and an imine N atom (N2) are situated trans to each other. In contrast, **3b** exhibits trans imine N atoms (N1 and N2), a representative architecture in many hexacoordinate Si complexes with two (O,N)-donor chelates.[14] In both complexes the (iminomethyl)phenolate ligands reveal similar strengths of coordination, since in **3a** as well as in **3b** the sums of the shorter Si−N(amide) and longer Si−N(imine) and the Si−O bonds, respectively, are similar.[12]

In case of **3a** and **3b**, respectively, ^{29}Si NMR spectra reveal similar coordination patterns of the Si atoms in chloroform solution and in the solid state (**3a**, δ −177.2 in $CDCl_3$ and δ −177.1 in the solid state; **3b**, δ −179.3 in $CDCl_3$ and δ −178.9 in the solid state).

To obtain more spectroscopic information about the colored complexes **3a** and **3b**, respectively, UV/vis spectra of the ligands used, and the spectrum of another complex with a *mer-fac* salen-type ligand (**I**) as well as those of **3a** and **3b** were

(9) Wagler, J.; Roewer, G. *Z. Naturforsch.* **2005**, *60b*, 709.

(10) Wagler, J.; Böhme, U.; Brendler, E.; Blaurock, S.; Roewer, G. *Z. Anorg. Allg. Chem.* **2005**, *631*, 2907.

(11) Schlosser, Th.; Sladek, A.; Hiller, W.; Schmidbaur, H. *Z. Naturforsch.* **1994**, *49b*, 1247.

(12) Crystal data for **3a**·2(dioxane) (CCDC-277626): triclinic, $C_{52}H_{56}N_4O_8Si$, M_r = 893.10, $P\bar{1}$, a = 12.618(1) Å, b = 13.826(1) Å, c = 14.102(1) Å, α = 96.355(10)°, β = 109.511(10)°, γ = 97.251(10)°, V = 2269.4(3) Å^3, T = 198(2) K, Z = 2, 7575 unique data ($2\theta \le 50°$), 632 parameters, R1($F^2 > 2\sigma(F^2)$) = 0.0399, wR2($F^2 > 2\sigma(F^2)$) = 0.0880, R1(all data) = 0.0853, wR2(all data) = 0.0999. Selected bond lengths (Å) and angles (deg): Si1−N1 = 1.989(2), Si1−N2 = 1.964(2), Si1−N3 = 1.833(2), Si1−N4 = 1.806(2), Si1−O1 = 1.786(1), Si1−O2 = 1.730(1); N1−Si1−O2 = 166.31-(6), N3−Si1−O1 = 172.90(7), N2−Si1−N4 = 172.14(8). Crystal data for **3b** (CCDC-277627): monoclinic, $C_{44}H_{42}N_4O_4Si$, M_r = 718.91, $P2_1/c$, a = 17.699(5) Å, b = 20.229(6) Å, c = 21.957(7) Å, β = 111.092(12)°, V = 7322(4) Å^3, T = 93(2) K, Z = 8, 12 880 unique data ($2\theta \le 50°$), 955 parameters, R1($F^2 > 2\sigma(F^2)$) = 0.0432, wR2($F^2 > 2\sigma(F^2)$) = 0.1093, R1-(all data) = 0.0748, wR2(all data) = 0.1203. Selected bond lengths (Å) and angles (deg): Si1−N1 = 2.006(2), Si1−N2 = 1.939(2), Si1−N3 = 1.827(2), Si1−N4 = 1.833(2), Si1−O1 = 1.766(2), Si1−O3 = 1.762(1); N1−Si1−N2 = 173.44(7), N3−Si1−O1 = 178.42(7), N4−Si1−O3 = 175.14(8).

(13) Seiler, O.; Burschka, C.; Fischer, M.; Penka, M.; Tacke, R. *Inorg. Chem.* **2005**, *44*, 2337.

(14) Kost, D.; Kalikhman, I. *Adv. Organomet. Chem.* **2004**, *50*, 1.

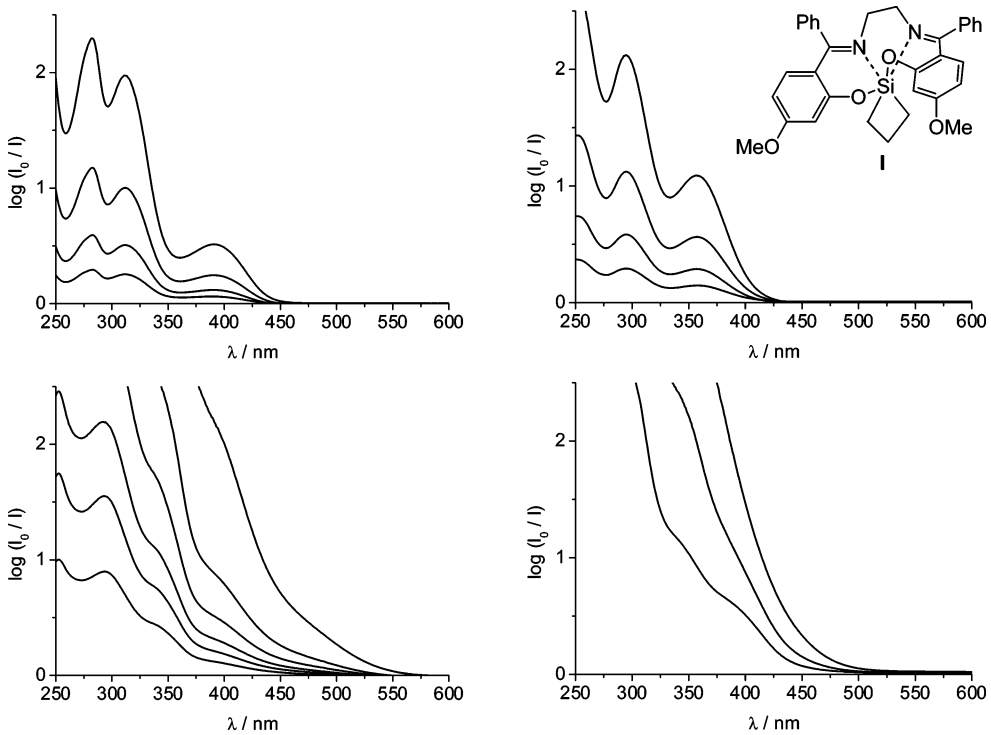

Figure 3. UV/vis spectra in chloroform ($d = 1$ mm) of (top left) ligand **2a** (0.13, 0.25, 0.50, 1.0 mmol/L); (top right) complex **I** (0.13, 0.25, 0.50, 1.0 mmol/L); (bottom left) **3a** (0.25, 0.50, 0.75, 1.0, 2.0, 5.0 mmol/L); (bottom right) **3b** (1.0, 2.0, 4.0 mmol/L).

recorded. As demonstrated in Figure 3, top, *mer-fac* coordination of ligand **2a** at the hexacoordinate silicon atom leads to a hypsochromic shift of its n→π* as well as π→π* absorption bands (λ_{max} (nm) (ϵ (L mol^{-1} cm^{-1})): for **2a**, 283 (23 600), 312 (20 200), 391 (4900); for **I**, 252 (29 700), 295 (23 500), 357 (11 600)). Although more than one n→π* transition has to be expected in the case of *mer-fac*-coordinated salen-like ligands, owing to different trans atoms relative to imine-N atoms, a splitting of the n→π* band was not observed in the spectrum of **I**. The extinction intensity of the n→π* absorption band of **I**, however, is significantly higher than that of **2a**. Ligand **2b** exhibits UV/vis absorptions similar to those of **2a** (λ_{max} (nm) (ϵ (L mol^{-1} cm^{-1})): for **2b**, 280 (10 300) 304 (11 400), 390 (5400)); thus, its spectrum is not depicted. Taking into account that **2b** represents half a molecule of **2a**, the extinction coefficients **2a**/**2b** should differ by a factor of 2. The n→π* transition of **2b** at 390 nm, however, emerges with much higher intensity. The difference of the symmetry of ligand **2a** in comparison with that of complex **I** and ligand **2b**, respectively, might be the reason for these stronger n→π* transitions in the last two compounds.

A hypsochromic shift of the tetradentate ligand's n→π* and π→π* absorption bands is also found in the spectrum of **3a** (Figure 3, bottom left) (λ_{max} (nm) (ϵ (L mol^{-1} cm^{-1})): for **3a**, 253 (40 000), 293 (35 000), 345 (shoulder) (15 000)). The larger hypsochromic shift of the n→π* absorption in comparison with that of **I** (compare the absorptions in the region 330−400 nm) is interpreted as being the consequence of a stronger coordination of the imine-N atoms' lone pairs to the Si atom with the more electronegative substituents, which is the case in compound **3a**. π→π* transitions of the diphenyldiazasilolidine moiety contribute to the strong absorptions below 300 nm. Intramolecular interligand charge transfer gives rise to additional absorption bands between 400 and 550 nm. (*N*,*N*′-diphenylethylenediamine has an absorption band at 296 nm ($\epsilon = 4150$ L mol^{-1} cm^{-1}), which is its UV feature of lowest energy). Due to the superposition of various weak bands, λ_{max} values cannot be estimated unambiguously from the measured spectra. The ϵ' coefficients of 1400 L mol^{-1} cm^{-1} at 450 nm and 500 L mol^{-1} cm^{-1} at 500 nm, however, represent absorption intensities with significantly increased magnitude in comparison with ligand **2a** (280 L mol^{-1} cm^{-1} at 450 nm and 0 L mol^{-1} cm^{-1} at 500 nm). Complex **3b** is extremely sensitive toward hydrolysis. For this reason, lowering the concentration below 1 mmol/L leads to the emergence of absorption bands of the educt **2b** in the UV/vis spectra of **3b**. Thus, although saturated in parts, only spectra of higher concentration were recorded and depicted in Figure 3 (bottom right). One can discern the same kind of low-energy absorptions as discussed for **3a**; however, there is a slight blue shift. Again, λ_{max} values cannot be estimated, due to the superposition of various weak absorption bands. The ϵ' coefficients at 450 nm are about 760 and 150 L mol^{-1} cm^{-1} at 500 nm, respectively (compare ligand **2b**: 200 L mol^{-1} cm^{-1} at 450 nm and 0 L mol^{-1} cm^{-1} at 500 nm).

Quantum chemical calculations with the time-dependent DFT method at the B3LYP/6-31+G* level of theory were applied to model the low-energy transitions creating the long wavelength part of the visible spectrum. They revealed the location of the highest occupied MOs, HOMO and HOMO-1, at the diazasilolidine moiety including significant participation of the amide nitrogen atoms in the formation of the respective MOs. In contrast, the lowest unoccupied MOs, LUMO and LUMO+1, are situated in the 2-(iminomethyl)phenolate parts of these complexes. The C═N moieties exhibit notable participation in setting up these MOs (Figures 4 and 5). Selected data for calculated singlet→singlet state electron transitions between these orbitals are given in Tables 1 and 2.

The silicon atoms are slightly involved in the composition of each of those molecular orbitals (between 1.8 and 3.5%). In the long-wavelength region separate absorption bands, such as those calculated for the HOMO→LUMO transition in **3a** at 635 nm, were not observed experimentally. Nevertheless, the measured intensely red shifted visible absorption up to about 600 nm in case of the saturated spectra of **3a** and the long-

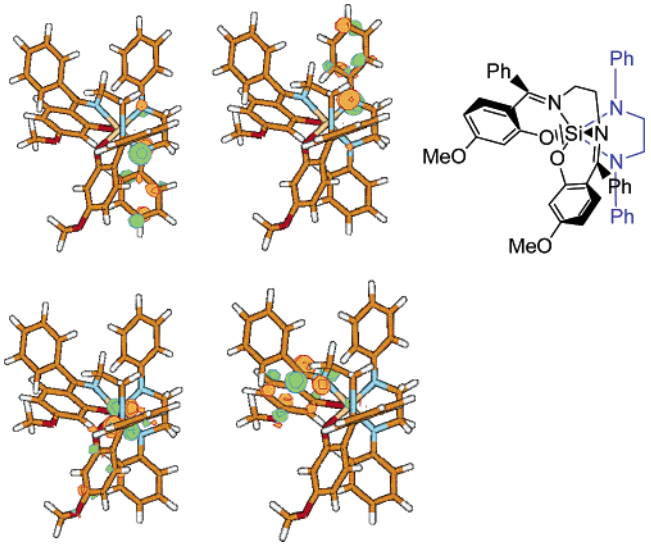

Figure 4. HOMO (top left), HOMO-1 (top middle), LUMO (bottom left), and LUMO+1 (bottom right) of **3a** (stick plots of molecule **3a**). The MOs are depicted with a contour value of 0.075 e Å^{-3}, and a sketch of **3a** to illustrate the perspective is given on the top right.

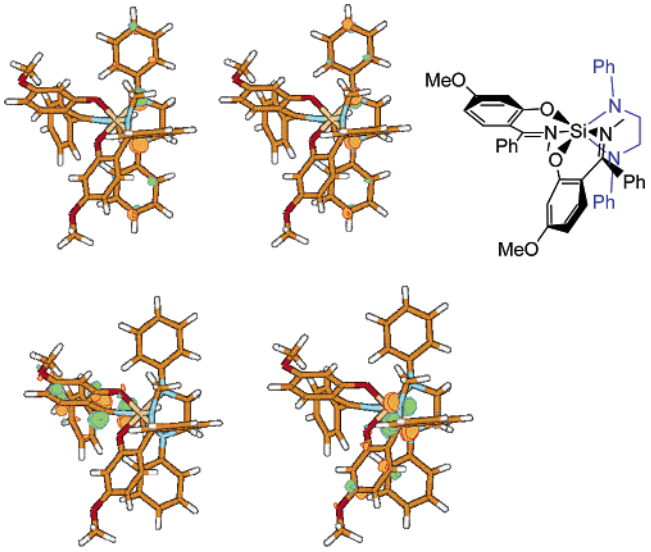

Figure 5. HOMO (top left), HOMO-1 (top middle), LUMO (bottom left), and LUMO+1 (bottom right) of **3b** (stick plots of molecule **3b**). The MOs are depicted with a contour value of 0.075 e Å^{-3}, and a sketch of **3b** to illustrate the perspective is given on the top right.

Table 1. Low-Energy Singlet Transitions Calculated for Molecule 3a[a]

MO	*c*	*E*/eV	*λ*/nm	*f*
HOMO→LUMO	0.6973	1.9538	635	0.0050
HOMO→LUMO+1	0.6971	2.2229	558	0.0031
HOMO-1→LUMO	0.6954	2.4969	497	0.0359

[a] Definitions: c = coefficient of the wave function for each excitation, f = oscillator strength.

wavelength absorption of **3b** were generally supported by quantum chemical methods. The results of those calculations confirm the intramolecular interligand charge transfer via the Si atom. Thus, we can conclude that in both cases the intense color is closely related to the donor−acceptor ligand situation at the Si atom. The trans arrangement of an imine and an amide N atom, however, may remarkably contribute to this charge transfer in **3a**. We can assume that the *mer-fac* ligand configuration of **3a** is retained in solution, since the number of ^{1}H and ^{13}C NMR signals in the spectrum indicate chemically nonequivalent halves of the salen-type ligand. Thus, the molecular orbital situation calculated for **3a** with *mer-fac*-arranged salen ligand should be relevant for the optical properties of **3a** in chloroform solution.

Table 2. Low-Energy Singlet Transitions Calculated for Molecule 3b[a]

MO	*c*	*E*/eV	*λ*/nm	*f*
HOMO-1→LUMO+1	0.1311	2.3373	530	0.0157
HOMO→LUMO	0.3949			
HOMO→LUMO+1	0.5660			
HOMO→LUMO	0.5784	2.3490	528	0.0101
HOMO→LUMO+1	−0.3914			
HOMO-1→LUMO	0.6983	2.6359	470	0.0035
HOMO-1→LUMO+1	0.6817	2.6751	463	0.0401
HOMO→LUMO+1	−0.1296			

[a] Definitions: c = coefficient of the wave function for each excitation, f = oscillator strength.

Both the LUMO and the LUMO+1 participate in the singlet transitions of **3b**. This is due to the nearly C_s symmetry of **3b**, which leads to very similar orbital energies in **3b**. (These two orbitals would be degenerate in an ideal C_s-symmetric molecule.) The energy gap between HOMO and HOMO-1 in **3b** is also notably smaller than in **3a**. Thus, some singlet transitions of **3b** involve contributions from more than two MOs (Table 2).

Conclusion

Compounds **3a** and **3b** represent a new motif tailored by Si hypercoordination. They are the first examples of single-component colored electron donor−acceptor devices in which the charge transfer between two units is mediated by a silicon atom. Charge transfer between donor and acceptor ligand moieties in complexes with "colorless" metal atoms is currently being intensively investigated. Those molecules, however, provide conjugated π-electron systems,[15] spacers with well established σ-delocalization,[16] or π-stacking between complex moieties.[17] Charge transfer in 4-donor- and 4′-acceptor-substituted diphenylsilanes has been reported.[18] This slight CT effect (UV required for excitation) cannot compete with the influence of donor and acceptor moieties on the visible spectra of the hexacoordinate Si complexes presented herein. Our results establish the ability of hypercoordinate silicon atoms to act as an electronic bridge helpful in tuning charge-transfer energies. Charge transfer via hypercoordinate silicon atoms may even open access to electronic surface manipulations on silicon wafers and in molecular electronic wires.

Experimental Section and Calculations

All of the following manipulations were carried out under an inert atmosphere of dry argon. THF and dioxane were distilled from sodium/benzophenone, and triethylamine was distilled from calcium hydride and stored over 3 Å molecular sieves. Chloroform (stabilized with amylene) was dried over 3 Å molecular sieves. NMR spectra were recorded on a Bruker DPX 400 ($CDCl_3$ solution

(15) (a) Zhang, T.-G.; Zhao, Y.; Asselberghs, I.; Persoons, A.; Clays, K.; Therien, J. M. *J. Am. Chem. Soc.* **2005**, *127*, 9710. (b) Kwak, G.; Fujiki, M.; Masuda, T. *Macromolecules* **2004**, *37*, 2422.

(16) Sharma, H. K.; Pannell, K. H.; Ledoux, I.; Zyss, J.; Ceccanti, A.; Zanello, P. *Organometallics* **2000**, *19*, 770.

(17) Ciliberto, E.; Doris, K. A.; Pietro, W. J.; Reisner, G. M.; Ellis, D. E.; Fragalà, I.; Herbstein, F. H.; Ratner, M. A.; Marks, T. J. *J. Am. Chem. Soc.* **1984**, *106*, 7748.

(18) van Walree, C. A.; Kooijman, H.; Spek, A. L.; Zwikker, J. W.; Jenneskens, L. W. *Chem. Commun.* **1995**, *1*, 35.

with TMS as internal standard) and a Bruker Avance 400 WB (CP/MAS spectra). Elemental analyses were carried out on a Foss Heraeus CHN-O-Rapid instrument. UV/vis spectra were recorded on a Specord S100 UV/vis spectrometer.

X-ray structure data for **3a** were recorded on a Bruker-Nonius KappaCCD diffractometer with Mo Kα radiation; data for **3b** were recorded on a Bruker-Nonius X8-APEX2-CCD diffractometer with Mo Kα radiation. The structures were solved with direct methods (SHELXS-97) and refined by least-squares methods (refinement of F^2 against all reflections with SHELXL-97). All non-hydrogen atoms were anisotropically refined. Hydrogen atoms were placed in idealized positions and refined isotropically.

The quantum chemical calculations were carried out using the GAUSSIAN 03 series of programs.[19] Geometries were fully optimized at the density functional theory level (DFT), using Becke's three-parameter hybrid exchange functional and the correlation functional of Lee, Yang, and Parr (B3LYP).[20,21] Geometry optimizations and harmonic frequencies were calculated with the polarized 6-31G* basis set for all elements.[22,23]

Excited-state energy calculations were performed with time-dependent DFT[24,25] at the B3LYP/6-31+G* level of theory using the optimized geometries.

Three-dimensional MO plots were generated with MOLDEN[26] with a contour value of 0.075 e Å^{-3} for all plots.

According to a previously published method,[27] ligands **2a** and **2b** were prepared in condensation reactions using 2-hydroxy-4-methoxybenzophenone and ethylenediamine or an ethanolic solution of methylamine, respectively. Synthesis of 1,1-dichloro-2,5-diphenyl-2,5-diazasilolidine (**1**) was described by Schmidbaur et al.[11]

3a. A mixture of THF (60 mL), triethylamine (2.00 g, 19.8 mmol), and ligand **2a** (2.50 g, 5.21 mmol) was stirred at 0 °C, and a solution of **1** (1.65 g, 5.34 mmol) in THF (35 mL) was added dropwise over a period of 30 min. The resulting orange mixture was stirred for a further 10 min, and then the triethylamine hydrochloride was filtered off and washed with THF (30 mL). The volume of the filtrate was reduced to ca. 50 mL by vacuum evaporation. After 4 days the orange-red crystalline product (**3a**·2THF) was filtered off, washed with THF (5 mL), and dried under vacuum. Yield: 2.20 g (2.56 mmol, 49%). Anal. Calcd for $C_{52}H_{56}N_4O_6Si$: C, 72.53; H, 6.55; N, 6.51. Found: C, 72.37; H, 6.35; N, 6.57.

Crystals of **3a**·2(dioxane) for X-ray analysis were obtained by recrystallization from dioxane.

Anal. Calcd. for $C_{52}H_{56}N_4O_8Si$: C, 69.93; H, 6.32; N, 6.27. Found: C, 69.68; H, 6.33; N, 6.15. ^{1}H NMR ($CDCl_3$): δ 2.3−2.4, 2.7−2.8, 3.05−3.15, 3.25−3.35 (4m, 4H, C═NCH_2CH_2N═C), 3.35−3.55 (m, 4H, PhNCH_2CH_2NPh), 3.56, 3.95 (2s, 6H, OMe), 5.75 (d, 1H, ar, $^4J_{HH}$ = 2.4 Hz), 5.94 (dd, 1H, ar, $^3J_{HH}$ = 9.2 Hz, $^4J_{HH}$ = 2.4 Hz), 6.30−7.65 (mm, 24H, ar). ^{13}C NMR ($CDCl_3$): δ 44.2, 46.1 (PhN*C*H_2*C*H_2NPh), 47.4, 49.1 (C═N*C*H_2*C*H_2N═C), 55.2, 55.6 (OMe), 104.5, 105.5, 107.5, 107.7, 113.0, 114.5, 115.0, 115.5, 115.9, 116.5, 117.9, 125.8, 126.8, 127.0, 128.5, 128.8, 129.9, 129.3, 129.4, 130.3, 130.8, 132.3, 133.9, 135.0, 135.4 (ar), 152.1, 152.4 (ar, C−N), 163.9, 164.9, 165.9, 166.0 (ar, C−O), 172.8, 173.1 (C═N). ^{29}Si NMR: δ −177.2 ($CDCl_3$), −177.1 (CP/MAS).

3b. Ligand **2b** (2.81 g, 11.7 mmol) was dissolved in THF (30 mL), and a solution of $NaN(SiMe_3)_2$ (2.15 g, 11.7 mmol) in THF (20 mL) was added dropwise. After 30 min the volatiles were removed under vacuum and the solid residue was dissolved in THF (20 mL). A solution of **1** (1.80 g, 5.83 mmol) in THF (30 mL) was then added dropwise. After 1 day the precipitated NaCl was filtered off. The volume of the filtrate was reduced under vacuum to 20 mL, and the orange solution was stored at 7 °C. After 2 weeks, the orange crystalline product was filtered off, washed with THF (3 mL), and dried under vacuum. Yield: 1.94 g (2.70 mmol, 46%). Mp (sealed capillary, not corrected): 153 °C. Anal. Calcd for $C_{44}H_{42}N_4O_4Si$: C, 73.51; H, 5.89; N, 7.79. Found: C, 73.36; H, 6.14; N, 8.06. Compound **3b** generates some broad signals in ^{1}H and ^{13}C NMR due to configurational inversion. ^{1}H NMR ($CDCl_3$): δ 3.07 (s, 6H, $-CH_3$), 3.52 (s broad, 4H, PhNCH_2CH_2NPh), 3.65 (s, 6H, OMe); 5.9−7.55 (mm broad, 26H, ar). ^{13}C NMR ($CDCl_3$): δ 40.6 (NCH_3), 46.2 (NCH_2CH_2N), 55.1 (OMe), 104.6, 106.3, 114.7, 117.0, 127.4, 127.8, 128.7, 129.2, 133.2, 136.8 (superposition of broad signals not resolved, ar), 152.6 (ar, C−N), 164.4 (2 signals, ar, CO), 173.9 (C═N). ^{29}Si NMR: δ −179.3 ($CDCl_3$), −178.9 (CP/MAS).

Acknowledgment. This work was financially supported by the German Chemical Industries Fund and the German Science Foundation (DFG). We thank Sigrid Goutal (Institut für Organische Chemie, TU Dresden, Dresden, Germany) for the X-ray structure analysis of **3a**.

Supporting Information Available: Crystallographic data of **3a** and **3b** as well as planarized sketches of the MOs discussed in this paper. This material is available free of charge via the Internet at http://pubs.acs.org.

OM050816E

(19) Frisch, M. J.; Trucks, G. W.; Schlegel, H. B.; Scuseria, G. E.; Robb, M. A.; Cheeseman, J. R.; Montgomery, J. A., Jr.; Vreven, T.; Kudin, K. N.; Burant, J. C.; Millam, J. M.; Iyengar, S. S.; Tomasi, J.; Barone, V.; Mennucci, B.; Cossi, M.; Scalmani, G.; Rega, N.; Petersson, G. A.; Nakatsuji, H.; Hada, M.; Ehara, M.; Toyota, K.; Fukuda, R.; Hasegawa, J.; Ishida, M.; Nakajima, T.; Honda, Y.; Kitao, O.; Nakai, H.; Klene, M.; Li, X.; Knox, J. E.; Hratchian, H. P.; Cross, J. B.; Bakken, V.; Adamo, C.; Jaramillo, J.; Gomperts, R.; Stratmann, R. E.; Yazyev, O.; Austin, A. J.; Cammi, R.; Pomelli, C.; Ochterski, J. W.; Ayala, P. Y.; Morokuma, K.; Voth, G. A.; Salvador, P.; Dannenberg, J. J.; Zakrzewski, V. G.; Dapprich, S.; Daniels, A. D.; Strain, M. C.; Farkas, O.; Malick, D. K.; Rabuck, A. D.; Raghavachari, K.; Foresman, J. B.; Ortiz, J. V.; Cui, Q.; Baboul, A. G.; Clifford, S.; Cioslowski, J.; Stefanov, B. B.; Liu, G.; Liashenko, A.; Piskorz, P.; Komaromi, I.; Martin, R. L.; Fox, D. J.; Keith, T.; Al-Laham, M. A.; Peng, C. Y.; Nanayakkara, A.; Challacombe, M.; Gill, P. M. W.; Johnson, B.; Chen, W.; Wong, M. W.; Gonzalez, C.; Pople, J. A. *Gaussian 03*, revision C.02; Gaussian, Inc.: Wallingford, CT, 2004.

(20) Becke, A. D. *J. Chem. Phys.* **1993**, *98*, 5648.

(21) Stevens, P. J.; Devlin, F. J.; Chablowski, C. F.; Frisch, M. J. *J. Phys. Chem.* **1994**, *98*, 11623.

(22) Hariharan, P. C.; Pople, J. A. *Theor. Chimica Acta* **1973**, *28*, 213.

(23) Francl, M. M.; Pietro, W. J.; Hehre, W. J.; Binkley, J. S.; Gordon, M. S.; DeFrees, D. J.; Pople, J. A. *J. Chem. Phys.* **1982**, *77*, 3654.

(24) Bauernschmitt, R.; Ahlrichs, R. *Chem. Phys. Lett.* **1996**, *256*, 454.

(25) Stratmann, R. E.; Scuseria, G. E.; Frisch, M. J. *J. Chem. Phys.* **1998**, *109*, 8218.

(26) Schaftenaar, G.; Noordik, J. H. *J. Comput.-Aided Mol. Design* **2000**, *14*, 123.

(27) Dinjus, U.; Stahl, H.; Uhlig, E. *Z. Anorg. Allg. Chem.* **1980**, *464*, 37.